

Pseudothreshold or threshold? – More realistic threshold estimates for fault-tolerant quantum computing

Krysta M. Svore,^{1,*} Andrew W. Cross,^{2,†} Isaac L. Chuang,^{2,‡} and Alfred V. Aho^{3,§}

¹*Columbia University, Dept. of Computer Science, 1214 Amsterdam Ave. MC:0401, New York, NY 10027*

²*Massachusetts Institute of Technology, Dept. of Electrical Engineering, 77 Massachusetts Ave., Cambridge, MA 02139*

³*Columbia University, Dept. of Computer Science, 1214 Amsterdam Ave. MC:0401, New York, NY 10025*

(Dated: December 13, 2018)

An arbitrarily reliable quantum computer can be efficiently constructed from noisy components using a recursive simulation procedure, provided that those components fail with probability less than the fault-tolerance threshold. Recent estimates of the threshold are near some experimentally achieved gate fidelities. However, the landscape of threshold estimates includes pseudothresholds, threshold estimates based on a single component and a single application of the recursive procedure. In this paper, we define pseudothresholds and present classical and quantum fault-tolerant circuits exhibiting pseudothresholds that differ significantly from fault-tolerance thresholds. Pseudothresholds are a generic phenomenon in fault-tolerant computation and recent quantum threshold estimates may in fact be pseudothresholds. We develop tools for visualizing the distinction between pseudothresholds and fault-tolerance threshold. Finally, we conjecture that refinements of these methods may establish upper bounds on the fault-tolerance threshold.

PACS numbers: 03.67.Lx, 03.67.Pp

Keywords: quantum computation, fault tolerance

I. INTRODUCTION

A quantum computer can potentially solve certain problems more efficiently than a classical computer [1, 2, 3]. However, quantum computers will need to be engineered from inherently noisy components, so any scalable quantum computer system will require quantum error correction and fault-tolerant methods of computation. As candidate quantum device technologies mature, we need to determine the component failure probabilities necessary to achieve scalability. The fault-tolerance threshold for gate and memory components is particularly interesting because arbitrarily reliable computations are possible if the circuit components have failure rates below the threshold. Given detailed knowledge of the fault-tolerance threshold and its associated tradeoffs, proposals for fault-tolerant quantum computation can be critically evaluated.

The concept of a fault-tolerance threshold has origins in the classical theory of computation. In the 1950’s, von Neumann showed that it is possible to achieve a reliable classical computation with faulty components provided that the failure probability of each component is below some constant threshold probability that is independent of the circuit size and the desired noise rate [4]. Similarly, concatenated coding and recursive error correction can be used to achieve reliable quantum computation. Concatenation is the process of encoding physical bits of one code as logical bits of another code. It is now well-known that using a single-error-correcting concatenated coding scheme with L levels of recursion, the maximum failure probability γ_{circuit} of a fault-tolerant circuit can be estimated as a function of the maximum failure probability γ of a basic component using the *fault-tolerance threshold inequality*

$$\frac{\gamma_{\text{circuit}}(\gamma)}{\gamma_{\text{th}}} \leq \left(\frac{\gamma}{\gamma_{\text{th}}} \right)^{2^L}, \quad (1)$$

where γ_{th} is the asymptotic threshold [5]. When Eq (1) holds with equality, we call it the *fault-tolerance threshold equation*. The final circuit failure probability γ_{circuit} decreases as a doubly exponential function of L if $\gamma < \gamma_{\text{th}}$.

One branch of fault-tolerant quantum computing research has focused on estimating the fault-tolerance threshold in the fault-tolerance threshold inequality. Figure 1 shows quantum threshold estimates that vary between 10^{-6} and 10^{-2} [5, 6, 7, 8, 9, 10, 11, 12, 13, 14, 15, 16]. The methods leading to these threshold estimates include numerical Monte-Carlo simulations and various analytical techniques. Numerical simulations can provide precise estimates, but only for the simplest noise models and

*Electronic address: kmsvore@cs.columbia.edu

†Electronic address: awcross@mit.edu

‡Electronic address: ichuang@mit.edu

§Electronic address: aho@cs.columbia.edu

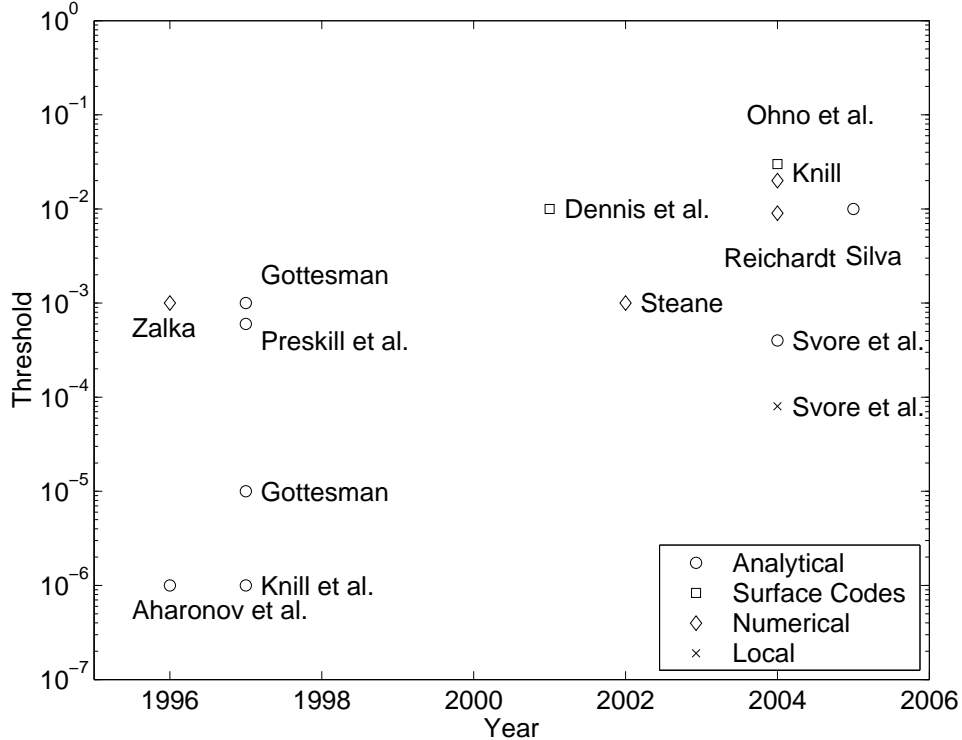


FIG. 1: Plots of quantum threshold estimates over recent years [5, 6, 7, 8, 9, 10, 11, 12, 13, 14, 15, 16]. Circles, squares, diamonds, and crosses respectively indicate estimates or bounds produced by: a) a counting analysis for CSS codes, b) an analysis for surface codes, c) numerical simulation, or d) a counting analysis for local computation with CSS codes. The mean reported threshold has tended to increase exponentially over the past several years due to improved fault-tolerance schemes and varied analysis methods. Some of these results have been based on the fault-tolerance threshold equation.

low levels of concatenation, since the computational effort in the simulations grows exponentially with concatenation level. On the other hand, analytical techniques can be used for high levels of concatenation, but they typically approximate or bound the threshold. The variability of the threshold estimates in Figure 1 is due both to differing analysis methods and gradually improved error correction techniques.

If there is a single type of component that is replaced uniformly, the fault-tolerance threshold inequality, Eq (1), becomes an equality. This leads to a very simple prediction shown in Figure 2(a): if $\gamma = \gamma_{th}$, then $\gamma_{circuit} = \gamma_{th}$. This fact is taken as the basis of many analyses of the fault-tolerance threshold today, because it implies that the threshold can be determined by finding the smallest nonzero value of γ that solves $\gamma_{circuit}(\gamma) = \gamma$. This simplification is particularly attractive for computationally expensive numerical simulations.

Realistically, however, the assumption of uniform replacement does not hold, so the first crossing point does not accurately indicate the fault-tolerance threshold. Figure 2(b) more accurately portrays the effect of recursive simulation. As the recursion level increases, for example, an exponentially growing number of wires must be introduced between gates. When these wires are unreliable, as they likely will be in quantum circuits, successive recursion levels can cause errors to increase even though γ is beneath the apparent threshold. Thus, recursive simulation changes the relative proportions of each type of component and what appears to be the threshold at one level of recursion may be far from the asymptotic threshold. This sequence of crossing points cannot be used to describe the proper conditions under which a system is scalable. Rather, these crossing points are pseudothresholds.

Nonuniform replacement treats each component differently, creating the opportunity for nontrivial engineering tradeoffs that still preserve scalability. Additional tradeoffs involving measurement and state preparation are possible in quantum computers. These tradeoffs can be quantified given the asymptotic threshold, families of pseudothresholds, and their relation to the shape of the set of subthreshold component parameters.

In this paper, we present methods for determining and distinguishing between pseudothresholds and asymptotic thresholds. We explore the conditions under which pseudothresholds exist and embark on this exploration carrying two tools. The first tool is a generalization of Figure 2(b), which we call the *threshold reliability information plot* (TRIP). In a TRIP, each curve represents the failure probability at concatenation level L and crosses the $L = 0$ line once. The crossing of a level- L curve and the level- $(L = 0)$ line yields the right-most edge of an interval on the γ -axis below which reliability is improved by concatenation. The

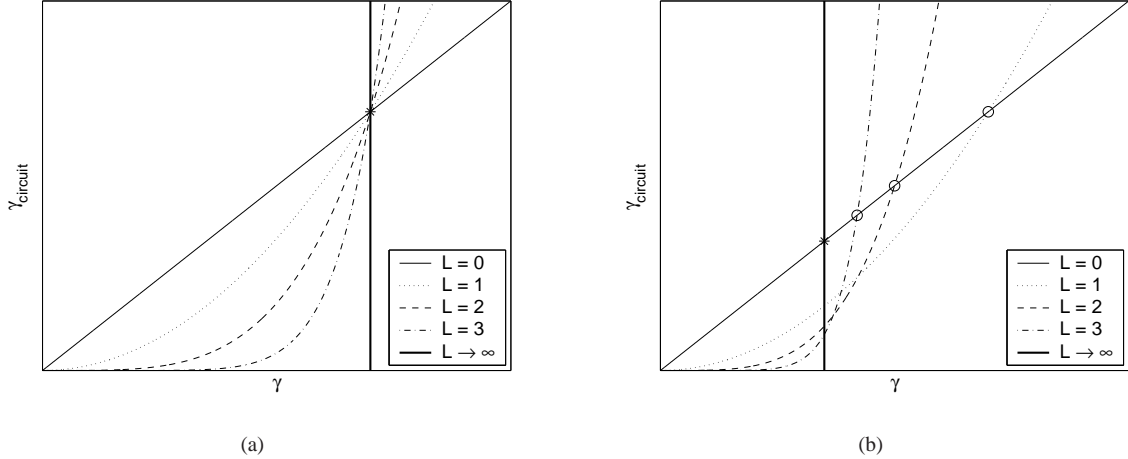


FIG. 2: (a) An ideal threshold reliability information plot (TRIP) follows Eq (1). The crossing point between the $L = 0$ line and the $L = 1$ curve, marked by asterisk on the thick vertical line, is the fault-tolerance threshold. All of the curves cross at the same point. (b) A real TRIP does not follow Eq (1). The crossing points between the $L = 0$ line and the other curves are all different. These points, marked by circles, correspond to a sequence of pseudothresholds that converges to the real fault-tolerance threshold marked by the asterisk on the thick vertical line.

crossing point is a level- L pseudothreshold.

The second tool is a *threshold information flow diagram* (TIFD) that shows how recursive simulation can change the reliability of a particular set of noisy components. A *flow* is a normalized vector field that can be visualized as a collection of arrows. Each arrow's base is anchored to a point that represents the current failure probability of the components. The direction of each arrow indicates the direction the anchor point moves at the next level of recursion. In contrast to the TRIP, the TIFD exposes how all of the component's failure probabilities change in a recursive simulation. If the recursive simulation is self-similar, particularly with respect to the noise model, then the TIFD indicates whether or not recursive simulation increases or decreases each component's failure probability, allowing us to observe the fault-tolerance threshold.

Figure 3 shows a TIFD for a hypothetical pair of faulty basic gates u and v . Because u and v compute different functions with differing degrees of interaction, their fault-tolerant implementations use different numbers of basic u and v gates. In this example, the fault-tolerant u contains two u gates and two v gates, connected in some fashion so that the fault-tolerant u can withstand one internal gate failure and still produce a “good” output. If basic gates u and v fail independently with probabilities γ_u and γ_v , respectively, then the failure probability of the fault-tolerant u gate is

$$1 - (1 - \gamma_u)^2(1 - \gamma_v)^2 - 2\gamma_u(1 - \gamma_u)(1 - \gamma_v)^2 - 2\gamma_v(1 - \gamma_v)(1 - \gamma_u)^2. \quad (2)$$

Similarly, the fault-tolerant v gate contains three u gates and three v gates and can withstand any single failure, giving

$$1 - (1 - \gamma_u)^3(1 - \gamma_v)^3 - 3\gamma_u(1 - \gamma_u)^2(1 - \gamma_v)^3 - 3\gamma_v(1 - \gamma_v)^2(1 - \gamma_u)^3. \quad (3)$$

There are many such hypothetical examples. In Section III, we give a more realistic example that demonstrates how a TIFD is calculated based on an actual circuit.

Continuing with this example, the effective failure probabilities of u and v after level-1 recursive simulation both depend on the initial failure probabilities γ_u^0 and γ_v^0 of u and v , shown on the horizontal and vertical axes of the TIFD. Consider the following scenario. The v gate initially fails with probability 0.2 and the u gate does not fail at all. A square marks this point on the TIFD. The arrow at this point on the TIFD points down and to the right, indicating that a level-1 recursive simulation will improve v but make u worse. The dashed line connects the initial failure probabilities to the failure probabilities of the level-1 simulated gates (at about (0.04, 0.1)). The dashed path shows that subsequent recursive simulation makes u and v arbitrarily reliable.

The TIFD in Figure 3 also indicates the set of initial failure probabilities that is below threshold. The boundary of this set is determined by a fixed point of the recursive simulation procedure. This fixed point is marked with a circle, and the thick dark line passing through this circle is the invariant set that indicates the fault-tolerance threshold. For example, an ideal v gate and a u gate that initially fails with probability 0.28 (marked by a square) is above threshold. This point flows nearly parallel to the invariant line at first, but ultimately escapes from the boundary of the TIFD after about 7 levels of recursive simulation.

We organize the paper as follows. In Section II, we first define the fault-tolerance threshold for concatenated flow equations, then we define pseudothresholds and describe their importance. We calculate, in Section III, a family of pseudothresholds

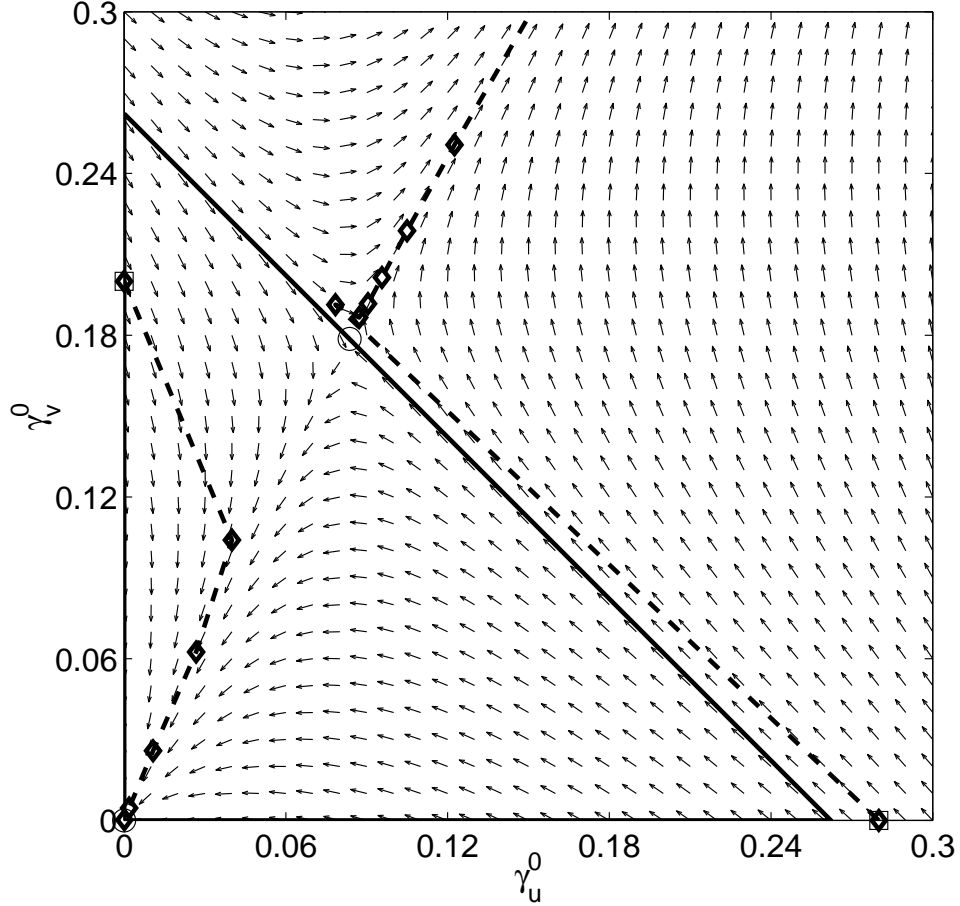


FIG. 3: Threshold information flow diagram (TIFD) corresponding to the following recursive simulation procedure: gates u and v at level- $(L-1)$ are both replaced by fault-tolerant gates at level L that can withstand a single level- $(L-1)$ gate failure. However, u and v compute different functions, so their fault-tolerant implementations are different. In this example, the fault-tolerant u contains two u gates and two v gates, and the fault-tolerant v contains three u gates and three v gates. Arrows on this TIFD indicate how the recursive simulation procedure changes the effective failure probabilities of u and v . For some failure probabilities, recursive simulation has no effect. These fixed points are marked by circles, and one of them determines the fault-tolerance threshold, indicated by a thick black line. Sample trajectories begin at the squares and flow along the thick dashed lines, where the diamonds mark the sequence of points for each level L of concatenation.

and distinguish them from the fault-tolerance threshold estimate for the classical repetition code. In Section IV, we study the $[[7, 1, 3]]$ CSS code, again comparing the fault-tolerance threshold against families of pseudothresholds. We suggest techniques for finding the threshold in Section V that expand upon our use of the TIFD. We conclude in Section VI with open questions.

II. PSEUDOTHRESHOLDS

In Section I, we discussed the phenomena of pseudothresholds, but what exactly are pseudothresholds and why do they occur? Although Eq (1) approximates the behavior of a fault-tolerant circuit, a closer estimate of the threshold for a given error model and error correction scheme requires a flow equation for each circuit component. These flow equations lead to a sequence of crossing points, as in Figure 2(b), that are pseudothresholds. In this section, we define both the fault-tolerance threshold and the pseudothreshold sequences for a set of flow equations.

A. The fault-tolerance threshold

The fault-tolerance equation (Eq (1)) does not model all of the resource requirements needed to achieve scalability in a quantum computer. As an equation with a single parameter, γ , it does not account for the tradeoffs between system components

that need to be understood to engineer a scalable quantum system. Even when location types, such as gates, measurements, and waiting qubits, are assigned different failure probabilities, a model of how to replace each component type is still required for an asymptotic threshold estimate to be close to the actual asymptotic threshold.

The threshold is related to the number of nonsparses (i.e. bad) fault paths through a circuit. Assume faults occur at discrete locations and times with probability dependent on the location type. The failure probability of the circuit can then be determined as a function of failure probabilities of types of locations. For a code correcting t errors, the probability that one of these bad fault paths occurs is no more than $C\gamma^{t+1}$, where γ is the largest failure probability of any type of location in the circuit and C is the number of ways to choose $t+1$ failed locations out of N total locations. The fault-tolerance threshold satisfies

$$\gamma_{th} \geq \left(\frac{1}{C}\right)^{1/(t+1)}, \quad (4)$$

since γ_{th} is the fixed point of the map $\gamma_{circuit}(\gamma) = C\gamma^{t+1}$.

Though correct, Eqn (4) does not account for the fact that different types of locations must be replaced differently under concatenation. Although different location types could have been assigned different failure probabilities, each type of location is modeled by the same $(t+1)$ st degree replacement under concatenation of the map. Specifically, the two-qubit gate is replaced in the same way as a one-qubit gate, when in fact a two-qubit gate requires around twice the error correction circuitry as a one-qubit gate.

The first step toward differentiating between location types, i.e. between gates, measurements, and waiting qubits, is to give each location type its own failure probability γ_ℓ where ℓ labels the location type. By choosing a particular setting of the γ_ℓ , such as $\gamma_\ell = \gamma/10$ if γ_ℓ is a waiting qubit and $\gamma_\ell = \gamma$ otherwise, for some free parameter γ , again $\gamma_{circuit}(\gamma)$ can be artificially treated like a one-dimensional map [15].

However, the fault-tolerant implementations of each location type differ, so in addition to assigning different failure probabilities to different location types, we must also express the failure probability of each fault-tolerant location type as a function of the location types it contains. In other words, we construct (approximations to) the *flow equations* for the given fault-tolerant implementations and noise model [6, 9]. In particular, if each type of location ℓ is assigned an initial failure probability γ_ℓ^0 and if there are n different types of locations, the approximate failure probability of location type ℓ after one level of recursive simulation is a function Γ_ℓ of all n of the initial failure probabilities. Therefore, Γ_ℓ is called the *flow equation for location type ℓ* .

All together, the functions Γ_ℓ are the coordinates of a *flow map* Γ . The flow map takes the failure probabilities of the n location types into their new values after one level of recursive simulation. The failure probabilities of the L -simulated location types are approximately related to the initial failure probabilities γ_ℓ^0 by the composed flow map,

$$\Gamma^L \equiv \underbrace{\Gamma \circ \cdots \circ \Gamma}_{L \text{ times}}. \quad (5)$$

Let Γ_ℓ^L denote the coordinate function of Γ^L associated with location ℓ , and let Γ_ℓ^0 be the initial function that selects the ℓ coordinate. In other words, Γ_ℓ^L approximates the failure probability of location ℓ after L levels of recursive simulation. The function Γ_ℓ^L is a *concatenated flow equation*, and the map Γ^L is the *concatenated flow map*. The concatenated flow map approximates the combined effect of all location types on the failure probability of L -simulated circuits.

A vector of failure probabilities $\vec{\gamma}$ for the n location types is *below threshold* if all n of the failure probabilities approach zero as the concatenation level approaches infinity,

$$\lim_{L \rightarrow \infty} \Gamma^L(\vec{\gamma}) = \vec{0}. \quad (6)$$

Let T be the set of these vectors that are below threshold, and let C_ϵ be the n -dimensional cube of edge length ϵ with one corner at the origin,

$$C_\epsilon \equiv \{\vec{\gamma} \in [0, 1]^n \mid \vec{\gamma}_\ell < \epsilon \ \forall \ell, \epsilon \in (0, 1]\} \quad (7)$$

The cube contains all of the vectors whose worst failure probability is less than ϵ . The *fault-tolerance threshold* or *asymptotic threshold* is the size of the largest cube contained in T , i.e.

$$\gamma_{th} \equiv \sup\{\epsilon \geq 0 \mid C_\epsilon \subseteq T\}. \quad (8)$$

If all component failure probabilities are beneath this probability, then composing the flow equations reduces the failure probability arbitrarily close to zero.

B. Definition of pseudothresholds

In Section I, pseudothresholds were introduced as crossing points on a TRIP (Figure 2(b)). Pseudothresholds are mistaken for the fault-tolerance threshold γ_{th} when only the first crossing point is considered, resulting in an estimate that can differ significantly from the asymptotic threshold. Pseudothresholds arise from at least two sources: neglecting components of the flow map Γ and considering only a few levels of recursive simulation. Pseudothresholds can be found for each type of location and for each level L of recursive simulation. The most dramatic difference between a pseudothreshold and γ_{th} normally occurs for an $L = 1$ pseudothreshold.

Before we define pseudothresholds, we introduce the concept of a *setting*. Settings parameterize a set of location failure probabilities by a single parameter so that we can think of Γ_ℓ^L as a function of this parameter. A setting is a function from a single failure probability parameter to a vector of n failure probabilities, one for each location. For example, the *diagonal setting* $g(\gamma) = (\gamma, \dots, \gamma)$ is used in analyses that assign each location the same initial failure probability. The *Steane setting* $g(\gamma)$ is another setting that sets all location failure probabilities to γ except for an waiting bit which is assigned $\gamma/10$ [15].

Suppose there are n types of locations. We define a pseudothreshold $\gamma_{\ell,g}^L$ for a fixed level of recursion $L > 0$, a location ℓ , and a setting g as the least nonzero solution to

$$\Gamma_\ell^L(g(\gamma)) = \gamma, \quad (9)$$

This definition presents the (L, ℓ, g) -pseudothreshold as a fixed-point calculation for a function derived from the flow map Γ . The left-hand size of Eq (9) can be viewed as one of the curves plotted in Figure 2(a), and the right hand size can be viewed as the $L = 0$ line. The point where these curves intersect is a pseudothreshold.

For fixed location ℓ and setting g , the sequence $\gamma_{\ell,g}^L$ is not necessarily constant as a function of L . In fact, the sequence is typically not constant, meaning that pseudothresholds are a generic phenomenon. More specifically, let γ_0 be any pseudothreshold of the flow map Γ for a setting g , and let $\vec{\gamma}_0$ be the constant vector $(\gamma_0, \dots, \gamma_0)$. The pseudothreshold γ_0 is independent of location type and recursion level only if the setting satisfies $\Gamma(g(\gamma_0)) = \vec{\gamma}_0$ and $\vec{\gamma}_0$ is a fixed point of Γ .

Despite the fact that pseudothresholds are not thresholds, pseudothresholds are interesting because only a fixed level of recursive simulation will be used in practice. If the goal is to construct a reliable fault-tolerant location type ℓ , and all of the location types have the same initial reliability (i.e. $g(\gamma) = (\gamma, \dots, \gamma)$), then choosing γ to be less than the (L, ℓ, g) -pseudothreshold makes the L -simulated gate location type ℓ more reliable than the initial gate. However, some caution must be applied to pseudothresholds as well because the $(1, \ell, g)$ -pseudothreshold and the $(2, \ell, g)$ -pseudothreshold can be substantially different.

In the following sections, we present an illustrative example of classical pseudothresholds followed by a more detailed example of quantum pseudothresholds. We show by means of these examples that pseudothresholds are generic to all multiparameter maps. In addition, we highlight that threshold estimates should account for multiple location types and higher levels of code concatenation to achieve more realistic threshold results. We support our findings in the quantum setting with a Monte-Carlo simulation of the $[[7, 1, 3]]$ code.

III. CLASSICAL PSEUDOTHRESHOLDS FOR THE [3, 1, 3] CODE

In this section, we analyze a classical example to build intuition about the differences between pseudothresholds and thresholds and illustrate potential difficulties in identifying fault-tolerance thresholds in a quantum fault-tolerance setting. We study pseudothresholds for classical fault-tolerant components based on the [3, 1, 3] repetition code. We use the threshold reliability information plot (TRIP) of the [3, 1, 3] code to identify pseudothresholds. We then characterize the flow map for our classical example using a threshold information flow diagram (TIFD).

A. The [3, 1, 3] code and its failure probability map

In this example, the classical single-error-correcting [3, 1, 3] repetition code, also called triple modular redundancy (TMR), is used to encode a single bit in three bits by copying it three times. To make a fault-tolerant classical wire using this code, three location types $\Omega = \{w, v, f\}$ are required, where

- $w : \{0, 1\} \rightarrow \{0, 1\}$ defined by $w(a) = a$ is a *wire*.
- $v : \{0, 1\}^3 \rightarrow \{0, 1\}$ defined by $v(a, b, c) = ab \oplus bc \oplus ca$ is a *voter*.
- $f : \{0, 1\} \rightarrow \{0, 1\}^3$ defined by $f(a) = (a, a, a)$ is a *fanout*.

The superscripts above indicate the Cartesian product. The wire w is analogous to a waiting bit in a quantum fault-tolerance analysis, and the voter v and fanout f perform error correction.

A noisy version of each location type is defined as follows. A noisy wire flips the output bit with probability γ_w . A noisy voter incorrectly indicates the output bit with probability γ_v . For simplicity, we choose to model the fanout gate to be perfect (noiseless).

To recursively construct a fault-tolerant wire, *replacement rules* are used. A replacement rule is a pair $(b, R(b))$ where $b \in \Omega$ and $R(b)$ is a circuit over Ω that specifies how to replace a level- $(L - 1)$ location at level L . $R(b)$ is called the *replacement* of b and must preserve the functionality of the original location b . We construct the replacement rules to mirror replacement rules for quantum circuits, in which a circuit location is replaced by error correction followed by a fault-tolerant implementation of the location.

The following steps suggest how to ensure proper component connectivity for a code encoding a single bit. First, replace b directly by $D^{\otimes n_o} \circ R(b) \circ E^{\otimes n_i}$ where D and E are an ideal decoder and encoder. We must have $D \circ E$ equal to the identity gate on a single bit, where the open circle \circ denotes function composition. The numbers n_i and n_o are the number of input and output bits of b , respectively. After replacing each component in this manner, make a second pass over the circuit and replace all pairs $D \circ E$ by bundles of wires. Finally, replace the remaining encoders and decoders by respective fault-tolerant implementations of input preparation and output readout. The resulting circuit components will be properly connected, and the circuit will not contain decoding and re-encoding components (because those components are not fault-tolerant).

For this example, a wire w is replaced by error correction followed by a transversal implementation of the wire, i.e. a wire is applied to each bit of the encoded input, shown in Figure 4. Note the first dashed box indicates the classical error correction, which involves w , v , and f location types, and the second dashed box indicates the fault-tolerant implementation of the original location. Similarly, Figures 5(a) and 5(b) show the fault-tolerant replacement of v and f , respectively.

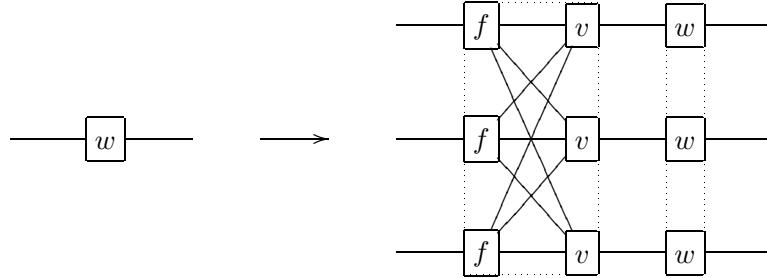


FIG. 4: Replacement rule for a wire w . The fanouts f and voters v perform error correction. The first dashed box indicates classical error correction using fanouts f and voters v . The second dashed box indicates the fault-tolerant implementation of the wire w .

Using the replacements $R(w)$ and $R(v)$, the failure probabilities $\Gamma_w(\vec{\gamma})$ and $\Gamma_v(\vec{\gamma})$ can be found, where the initial vector of failure probabilities is $\vec{\gamma} = (\gamma_w^0, \gamma_v^0)$. Failure is defined to be when the component's output does not decode to the correct value. The wire failure probability is easily calculated by counting the number of ways each configuration of errors occurs. For example, three voters fail in one way, three voters and one wire fail in three ways, two voters fail in three ways, etc. Rewriting the resulting polynomial in distributed form gives

$$\begin{aligned} \Gamma_w(\vec{\gamma}) = & 6\gamma_v\gamma_w + 3\gamma_v^2 + 3\gamma_w^2 - 2\gamma_v^3 - 18\gamma_v^2\gamma_w + 12\gamma_v^3\gamma_w - 18\gamma_v\gamma_w^2 \\ & + 36\gamma_v^2\gamma_w^2 - 24\gamma_v^3\gamma_w^2 - 2\gamma_w^3 + 12\gamma_v\gamma_w^3 - 24\gamma_v^2\gamma_w^3 + 16\gamma_v^3\gamma_w^3, \end{aligned} \quad (10)$$

where the superscript 0 is dropped for notational convenience.

Replacing the wire failure probability γ_w^0 by γ_v^0 and the voter failure probability γ_v^0 by the probability of error correction failure $3(\gamma_v^0)^2(1 - \gamma_v^0) + (\gamma_v^0)^3$ gives

$$\begin{aligned} \Gamma_v(\vec{\gamma}) = & 3\gamma_v^2 + 16\gamma_v^3 - 39\gamma_v^4 - 126\gamma_v^5 + 474\gamma_v^6 - 288\gamma_v^7 - 936\gamma_v^8 \\ & + 2080\gamma_v^9 - 1824\gamma_v^{10} + 768\gamma_v^{11} - 128\gamma_v^{12}, \end{aligned} \quad (11)$$

where the superscript is dropped again in the last expression.

The flow equations Eq (10) and Eq (11) are exact, even under composition, so they indicate the asymptotic threshold. They can also be used to determine a bound on the number of nonsparse fault paths, as discussed in Section II, by considering only the second-order terms in the flow equations:

$$\Gamma_w(\vec{\gamma}) \leq 3\gamma_w^2 + 3\gamma_v^2 + 6\gamma_w\gamma_v \quad (12)$$

$$\Gamma_v(\vec{\gamma}) \leq 3\gamma_v^2. \quad (13)$$

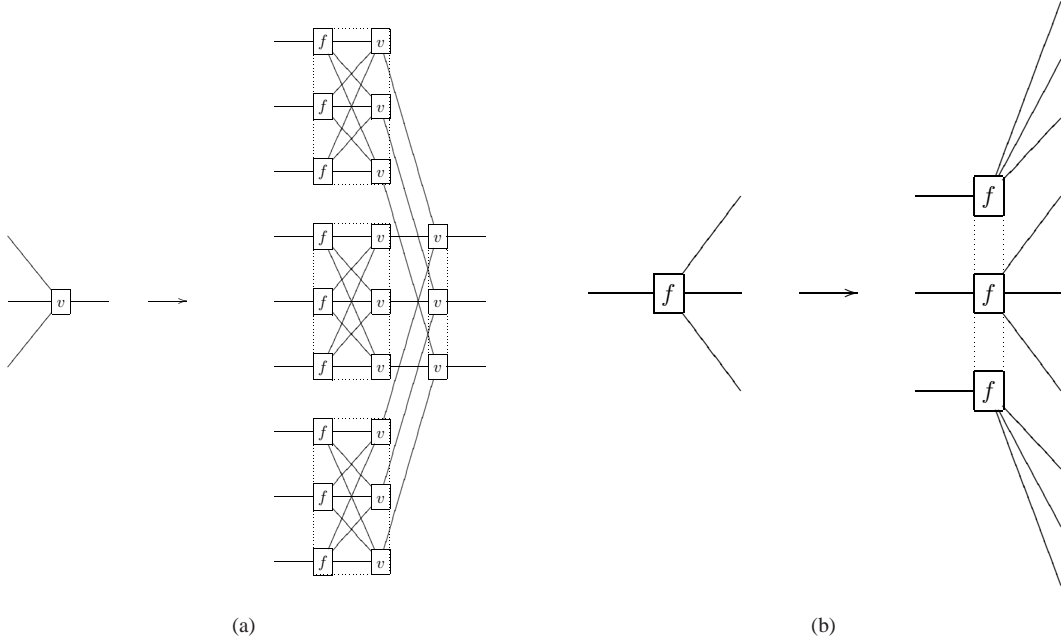


FIG. 5: (a) Replacement rule for a voter v . The first dashed box indicates classical error correction using fanouts f and voters v . The second dashed box indicates the fault-tolerant implementation of the voter v . (b) Replacement rule for a fanout f . Because we assume fanouts are perfect (noiseless), the replacement is just three fanout gates f .

These bounds clarify the relative contribution each component makes to the failure probability of a fault-tolerant component. They also suggest a conservative bound of $1/12$ on γ_{th} , calculated by adding the coefficients of each bound and taking the reciprocal of the worst. The waits pull the threshold toward $1/12$ while the voters push the threshold toward $1/3$.

B. TRIPs for the $[3, 1, 3]$ code

What is the behavior of the wire and voter failure probabilities as the concatenation level L increases? TRIPs based on Eqs (10)–(11) provide a visualization of each level crossing point for the two types of locations. Figures 6 and 7 are TRIPs for the voter and wire locations, respectively. From Figure 6, it is clear the voter probability $\Gamma_v(\vec{\gamma})$ is a one-parameter map, and thus should resemble the TRIP for the fault-tolerance threshold equation (Figure 2(a)). Since $\Gamma_v(\vec{\gamma})$ is a function of only γ_v^0 for all L , each $\Gamma_v^L(\vec{\gamma})$ intersects at the same fixed-point of the map. This fixed point γ_{th} , indicated by a thick vertical line, is the $L = \infty$ pseudothreshold and the asymptotic threshold. It occurs at approximately 0.246.

Surprisingly, even for a classical setting, there is a difference between pseudothresholds and the asymptotic threshold γ_{th} . Figure 7 shows the TRIP for the wire location at levels $L = 0, 1, 2, 3, \infty$. Here, unlike in the TRIP for the voter location, pseudothresholds appear in addition to an asymptotic threshold. This is because the replacement $R(w)$ for a wire includes locations of type w, v , and f , creating a two-parameter map (fanouts are noiseless) that exhibits changing behavior with each concatenation level L . The curves now cross the $L = 0$ line at different points. Each of these crossing points in the TRIP is a level- L pseudothreshold. As we repeatedly replace the wire using $R(w)$, the number of voter locations begins to dominate, so the crossing point approaches the asymptotic threshold. Even in the simplest classical setting, pseudothresholds appear. The difference between the fault-tolerance threshold $\gamma_{th} \approx 0.246$ and the level-1 wire location pseudothreshold $\gamma_w^1 \approx 0.129$ is a significant 48% of the asymptotic threshold.

C. TIFDs for the $[3, 1, 3]$ code

Given that pseudothresholds can be so different from γ_{th} , can γ_{th} be determined from just one application of the flow map? In Section I, it was suggested that a TIFD provides an informative view of the effect of recursive simulation. Although, a TRIP provides a visualization of the asymptotic behavior, it hides the fact that a single level of the map contains all of the information

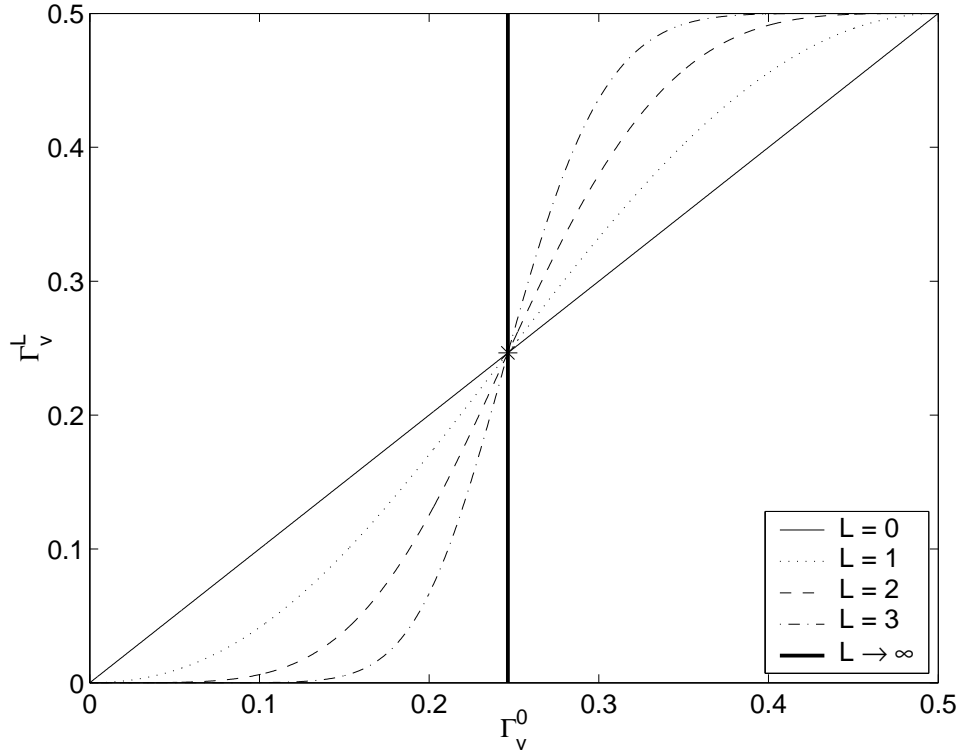


FIG. 6: TRIP for a voter location for the $[3, 1, 3]$ code for $L = 0, 1, 2, 3$. Because Γ_v^L is a function of only γ_v^0 constructed by recursive application of $R(v)$, all of the curves Γ_v^L intersect at the same point. This point is the fixed-point $\gamma_{th} \approx 0.246$ of the map and is indicated by an asterisk.

about the flow since the flow map is not level dependent. A TIFD, on the other hand, shows where each point flows under repeated application of the failure probability map without iterating the map explicitly.

In Figure 8, a TIFD for wire and voter failure probabilities on the unit half square is shown. The arrows represent the vectors $\Gamma(\vec{\gamma}) - \vec{\gamma}$, which give the probability flow under recursive simulation. Circles mark the fixed points of the map: $(0, 0)$, $(1/2, 0)$, $(1/2, \gamma_{th})$, $(1/2, 1/2)$, and $(1, 0)$, where $\gamma_{th} \approx 0.246$ cannot be expressed in radicals. The subthreshold region T is $[0, 1/2] \times [0, \gamma_{th}]$, indicated by the thick black box. Three corners of the subthreshold region are fixed points of the map. The fault-tolerance threshold γ_{th} is the size of the largest “cube”, a square in this case, that is contained in the subthreshold region.

First, if $\gamma_w^0 = 0$ and $\gamma_v^0 > 0$, then the flow draws these points off of the γ_v^0 -axis. This occurs because the wire replacement rule $R(w)$ contains both voter and wire locations, so the failure probabilities “mix”. Second, if $\gamma_v^0 = 0$, then any point $\gamma_w^0 < 1/2$ flows to the origin because the voters amplify any bias toward success. Third, the voter failure probability $\Gamma_v(\vec{\gamma})$ is independent of γ_w^0 , so the voter probability is a simple one-parameter map under replacement. If $\gamma_v^0 < \gamma_{th}$, the map’s fixed point, then the voter probability flows toward the γ_v^0 -axis. Finally, if $\gamma_v^0 < \gamma_{th}$ and $\gamma_w^0 < 1/2$, then initially the wire failure probability may increase because the voters are not reliably correcting errors. However, the voters improve with each iteration, so eventually this trend reverses. The voters begin correcting more errors than they introduce, and all of these points flow toward the origin.

For the classical $[3, 1, 3]$ code, the TIFD fully characterizes the threshold set T for three reasons. First, deviated inputs, i.e. inputs that are not codewords, are corrected before faults are introduced by the simulated gate locations. Second, the flow equations are the precise component failure probabilities. Third, there is no phase noise in classical fault-tolerance, so the parameters of the noise channel only change in the trivial way. Furthermore, the entire flow is easily visualized since the TIFD is two-dimensional. Under these conditions, the TIFD is an ideal tool for understanding and visualizing the process by which recursive simulation improves reliability and exhibits a threshold.

IV. QUANTUM PSEUDOTHRESHOLDS

Surprisingly, pseudothresholds exist even in a simple classical fault-tolerance scheme. In a quantum fault-tolerance scheme, the tools we have developed can now be applied to determine sequences of quantum pseudothresholds. In this section, we study thresholds for quantum fault-tolerance using the $[[7, 1, 3]]$ CSS code. We follow the circuit construction given in [15]. As in

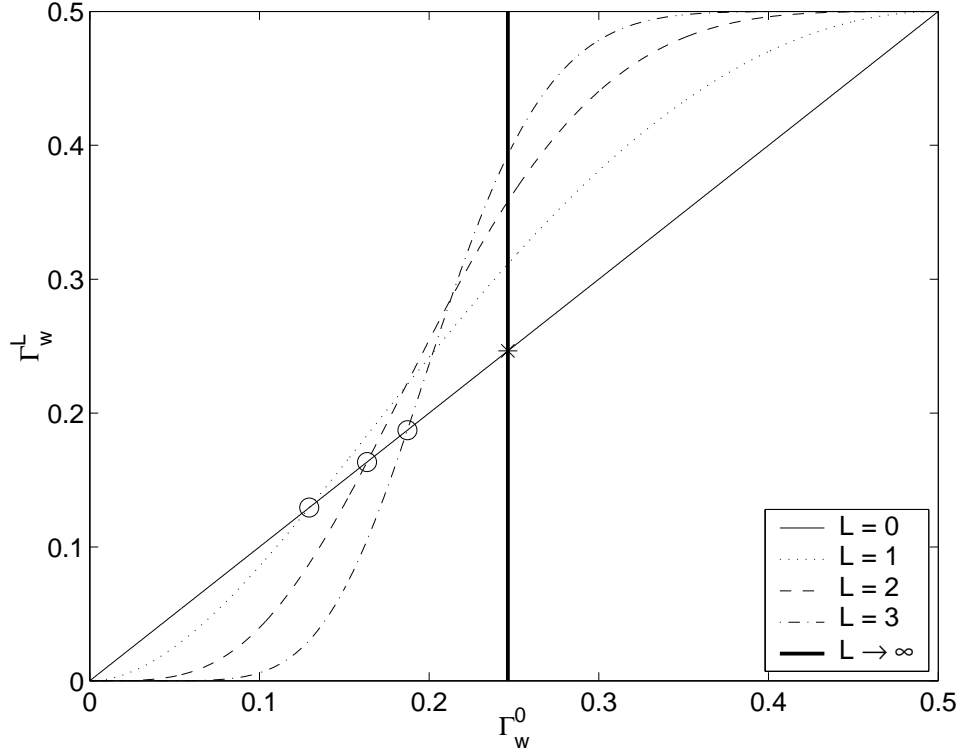


FIG. 7: TRIP for a wire location for the $[3, 1, 3]$ code for $L = 0, 1, 2, 3, \infty$ using the diagonal setting $\gamma_w^0 = \gamma_v^0$. Because Γ_w^L is a function of both γ_w^0 and γ_v^0 constructed by recursive composition, the curves Γ_w^L cross the $L = 0$ line at different points. Each of these points is a level- L pseudothreshold indicated by a circle, and the sequence of pseudothresholds $\gamma_w^1, \gamma_w^2, \dots$, converges to the fault-tolerance threshold $\gamma_{th} \approx 0.246$ indicated by an asterisk.

the classical example, TRIPs are again used to identify pseudothresholds for the given location types, allowing us to determine the reliability achieved with each level of concatenation. In addition, we characterize the failure probability map using TIFDs, which also allow us to find pseudothresholds.

A. The $[[7, 1, 3]]$ code and its flow map

The $[[7, 1, 3]]$ quantum code encodes a single qubit in 7 qubits with distance 3, meaning it corrects a general quantum error on a single qubit. The set of location types ℓ involved in the error correction routine is $\Omega = \{1, 2, w, 1m, p\}$:

- $\ell = 1$: one-qubit gate
- $\ell = 2$: two-qubit gate
- $\ell = w$: wait (memory) location
- $\ell = 1m$: one-qubit gate followed by measurement (see [6] for location type choice)
- $\ell = p$: ancilla preparation location, which we model as a one-qubit gate (see [6])

We consider the depolarizing error model, where a location ℓ fails with probability γ_ℓ . As in the classical case, we define a replacement rule for each type of location. We use the same replacement rules as given in [6], where we replace each location by error correction followed by a fault-tolerant implementation of the location. For example, a one-qubit gate is replaced by error correction and a transversal one-qubit gate, as shown in Figure 9.

We use the same approach as in the classical example, with the caveat that we do approximate counting of the failures following the failure probability map given in Section IV B of [6], where the composition of this map approximates the behavior of the concatenated circuit. This means that threshold results derived from this map are also approximate.

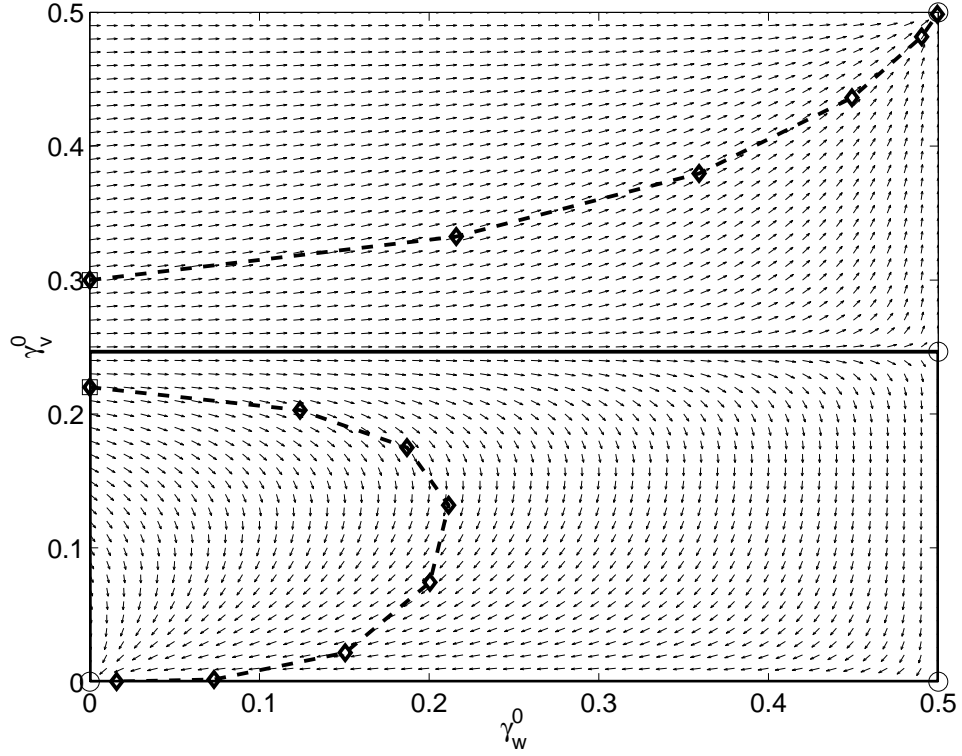


FIG. 8: TIFD for γ_w and γ_v for the $[3, 1, 3]$ code. The fixed points are indicated by circles. The region $[0, 1/2] \times [0, \gamma_{th}]$ enclosed by a thick line is the set of points below threshold, where $\gamma_{th} \approx 0.246$. Two sample trajectories begin at the squares and flow along the thick dashed lines, where the diamonds indicate the sequence of points as L increases, toward $(0, 0)$ and $(1/2, 1/2)$.

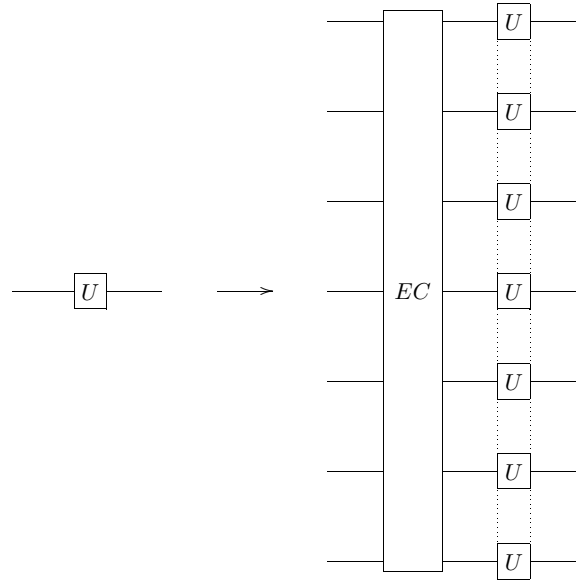


FIG. 9: Replacement rule for a one-qubit gate U . The replacement includes error correction (EC) followed by a fault-tolerant implementation of the one-qubit gate U , indicated by a dashed box.

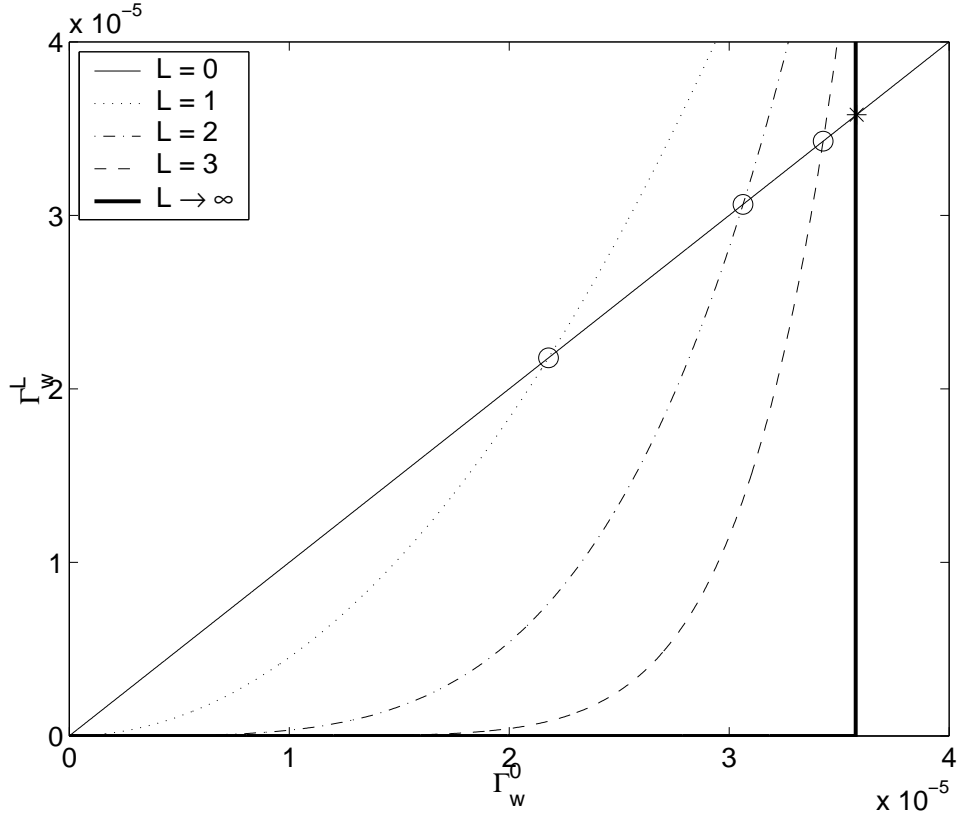


FIG. 10: TRIP for a wait location for $L = 0, 1, 2, 3, \infty$ for the initial setting $\gamma_w^0 = 1/10(\gamma_i^0)$, where i indicates all location types except for a wait location. Circles indicate pseudothresholds and an asterisk marks the fault-tolerance threshold.

B. TRIPs for the $[[7, 1, 3]]$ code

To determine pseudothresholds, we plot the reliability of each component at each level of concatenation using the flow equations. Figures 10–12 show TRIPs for wait, one-qubit, and two-qubit locations for the Steane setting $g(\gamma) = (\gamma, \gamma, \dots, \gamma, \gamma/10)$, where the last component is the wait location failure probability.

Figure 10 shows the TRIP for a wait location at levels $L = 0, 1, 2, 3, \infty$. Since the flow map is a multi-parameter map, the crossing points no longer cross the line $L = 0$ at the same point and thus pseudothresholds appear at each level. As L increases, the level- L pseudothreshold approaches an asymptotic threshold that depends on the location and setting. Note that the region between the $L = 1$ curve and the $L = 0$ line is quite small for these initial conditions, smaller than the region considered to be below the asymptotic threshold. This is similar to the behavior of the classical wait location. The behavior is largely due to the Steane setting – the level-1 simulation of the wait location includes other location types that have been set to fail with probability $10\gamma_w^0$. However, as the level of concatenation of the wait location increases, the trade-offs between the failure probabilities of the location types begins to stabilize causing the level-4 pseudothreshold, for example, to be much larger and closer to the asymptotic threshold.

Figure 11 shows the TRIP for the one-qubit location type for levels $L = 0, 1, 2, 3, \infty$. The level-1 pseudothreshold is around an order of magnitude worse than the level-4 pseudothreshold since the replacement $R(1)$ includes many wait locations, whose initial setting is one-tenth of the initial one-qubit gate failure probability.

Similarly, for a two-qubit gate location, the level-1 pseudothreshold is much larger than the higher-level pseudothresholds (Figure 12). Note that the level-1 pseudothreshold is about half the size of the level-1 one-qubit gate pseudothreshold. This is because error correction is required on two logical qubits and thus there are twice the number of locations in a one-qubit gate replacement.

From the threshold reliability information plots (TRIPs), it is apparent that multi-parameter maps and higher levels of concatenation are required to determine a threshold result. For some location types, the level-1 pseudothreshold is almost an order of magnitude larger than the asymptotic threshold. For the one-qubit gate, the level-1 pseudothreshold is near the fault-tolerance threshold found by Steane [15], potentially indicating that an asymptotic threshold was not found. Similarly, other recent results quote high fault-tolerance thresholds around $O(10^{-2})$, when in fact low levels of concatenation and few location types were ac-

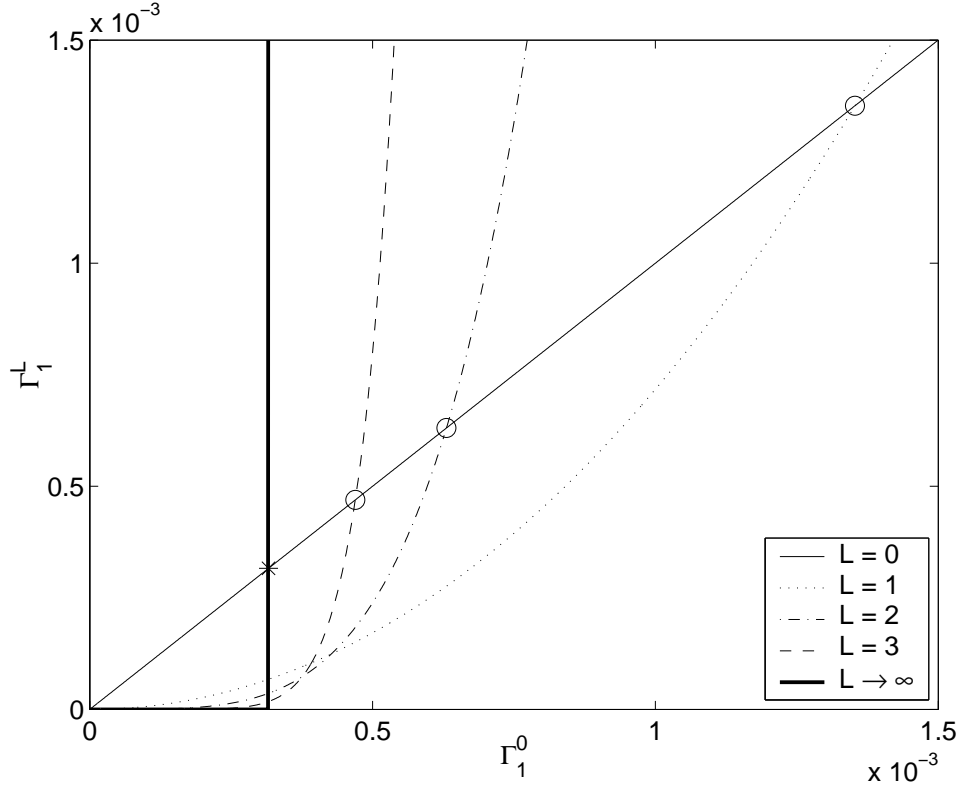


FIG. 11: TRIP for a one-qubit gate location for $L = 0, 1, 2, 3, \infty$ for the initial setting $\gamma_w^0 = 1/10(\gamma_i^0)$, where i indicates all location types except for a wait location. Circles indicate pseudothresholds and an asterisk marks the fault-tolerance threshold.

counted for in determining the fault-tolerance threshold results [11, 13]. More accurately, these values may be closer to level-1 pseudothresholds than an asymptotic threshold.

C. TIFDs for the $[[7, 1, 3]]$ code

We use the TIFD to characterize the flow of the maps based on the semi-analytical methods of [6]. By using a TIFD instead of the TRIP, the flow of the failure probabilities as well as pseudothresholds can be visualized. In the quantum case, however, the TIFD is a 4-dimensional flow that is challenging to visualize. Instead, we take 2-dimensional projections to determine the flow.

Figures 13–14 show TIFDs involving location types $l = 1, 2, w$. Figure 13 shows the vector field $\Gamma^L(\vec{\gamma}) - \Gamma^{L-1}(\vec{\gamma})$ projected onto the $\gamma_1 - \gamma_w$ plane. Note that the flows are partitioned by separatrices shown by the thick black lines. The map is independent of concatenation level in our approximation, so this flow fully characterizes the behavior of the map. The γ_1 threshold, found by the horizontal separatrix, appears around 1.1×10^{-4} . The asymptotic threshold for the map restricted to the γ_w -axis is indicated by an asterisk on the γ_w -axis. Note the separatrix indicates a wait location pseudothreshold.

Figure 14 is the TIFD projected onto the $\gamma_1 - \gamma_2$ plane. Again, the flows form a separatrix around $\gamma_2 = 2 \times \gamma_1$. This is because there are two error correction routines in a two-qubit gate replacement, compared to only one error correction routine in the replacement for a one-qubit gate. The γ_2 threshold appears along the other separatrix around 2.3×10^{-3} . The asymptotic threshold restricted to the γ_2 -axis, indicated by the asterisk, is a factor below the pseudothreshold.

In the classical setting, the TIFD indicated the asymptotic threshold, since the map was exact and only two-dimensional. However, it is evident from the TIFDs for the $[[7, 1, 3]]$ code that 2-dimensional projections of the flow are insufficient to determine the quantum fault-tolerance threshold set T . Since the threshold set is a multi-dimensional surface, the two-dimensional projection fails to indicate flow in the other dimensions. Although it appears the separatrices indicate a separation between points that flow to zero and those that flow to one, it cannot be used to determine the threshold, but it may be used to determine an upper bound on the threshold for this example.

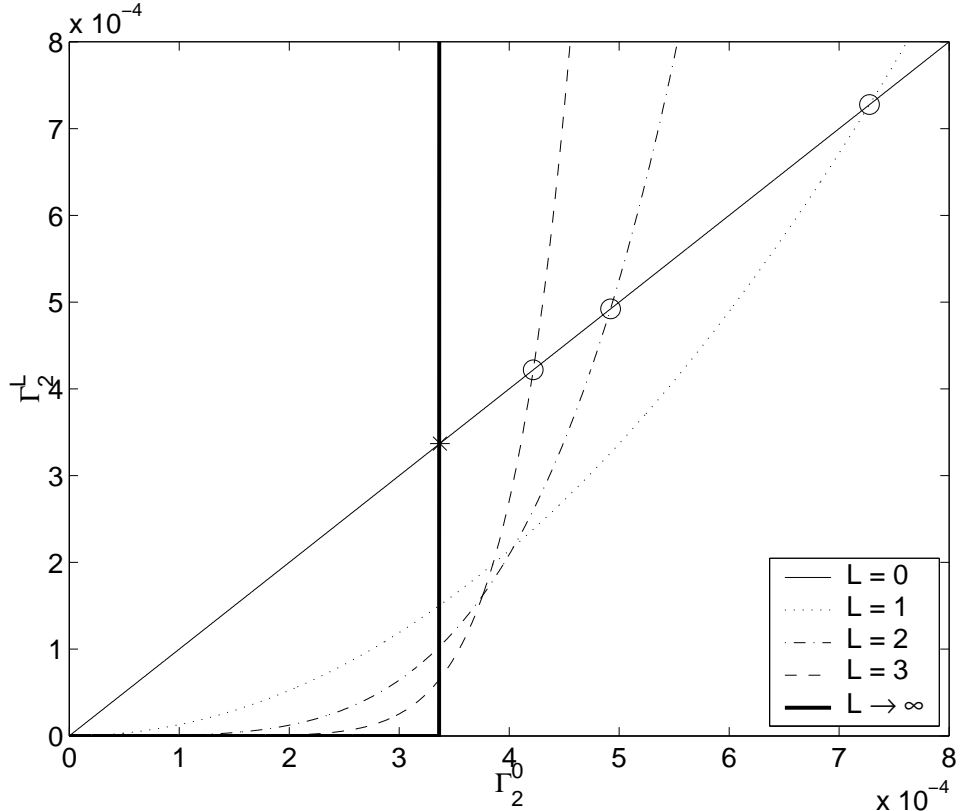


FIG. 12: TRIP for a two-qubit gate location for $L = 0, 1, 2, 3, \infty$ for the initial setting $\gamma_w^0 = 1/10(\gamma_i^0)$, where i indicates all location types except for a wait location. Circles indicate pseudothresholds and an asterisk marks the fault-tolerance threshold.

V. TECHNIQUES FOR DETERMINING THE ASYMPTOTIC THRESHOLD

In Section IV, low-dimensional projections of the flow using a TIFD were used to establish pseudothresholds. However, the TIFD could not be used to determine the asymptotic threshold γ_{th} . It may be possible, though, to bound γ_{th} by restricting the map Γ to the axes. In this section, we describe a possible technique for upper bounding the fault-tolerance threshold γ_{th} .

Consider the following setting, the *axis setting*, where every initial failure probability is 0, except for the axis of interest, i.e. $g(\gamma) = (\gamma, 0, 0, \dots, 0)$, and γ is assigned to the location axis of interest. We conjecture that the level-1 pseudothreshold for this setting upper bounds γ_{th} .

Consider the plot shown in Figure 15 of the approximated γ_w pseudothresholds of the $[[7, 1, 3]]$ code for the axis setting. Note that the pseudothresholds for the wait location for the axis setting are strictly decreasing toward a threshold. We find similar behavior for the other location types as well. These pseudothresholds and the threshold found for the wait location are lower than the pseudothresholds and thresholds for the other location types in the axis setting. This suggests that the $L = 1$ wait location pseudothreshold for the axis setting, the smallest level-1 axis pseudothreshold, is an upper bound on γ_{th} .

This conclusion that pseudothresholds with the axis setting provide an upper bound on the fault-tolerance threshold is supported by numerical evaluation of the threshold set T in Figure 16. This figure shows four convex hulls: one pseudothreshold hull and three threshold hulls. The pseudothreshold hull is determined by the γ_1^1, γ_2^1 , and γ_w^1 axis pseudothresholds, which are plotted as circles, while the threshold hulls were determined numerically from the flow map for a grid of parameters. The region of parameter space above the pseudothreshold hull is strictly above threshold. The largest threshold hull corresponds to $\gamma_{1m}^0 = 0$ and all points beneath it are below threshold. Similarly, the other two threshold hulls correspond to $\gamma_{1m}^0 = 1.5 \times 10^{-3}$ and $\gamma_{1m}^0 = 3.5 \times 10^{-3}$.

Interestingly, as our choice of language indicates, T appears to be a convex set equal to the convex hull of the axes thresholds and the origin. The edge length of the largest cube in T is approximately $\gamma_{th} \approx 8.8 \times 10^{-5}$. Furthermore, T appears to be contained in the convex hull of the axes pseudothresholds and the origin. These pseudothresholds are $\gamma_1^1 \approx 4.4 \times 10^{-2}$, $\gamma_2^1 \approx 2.3 \times 10^{-3}$, and $\gamma_w^1 \approx 1.1 \times 10^{-4}$. The γ_{1m}^1 pseudothreshold is comparable to γ_1^1 . The smallest level-1 pseudothreshold is $\gamma_w^1 \approx 1.1 \times 10^{-4}$, so this is an upper bound on γ_{th} for this example. Though the error correction networks are slightly different, this upper bound does not contradict a rigorous lower bound of 2.73×10^{-5} for the same code [17].

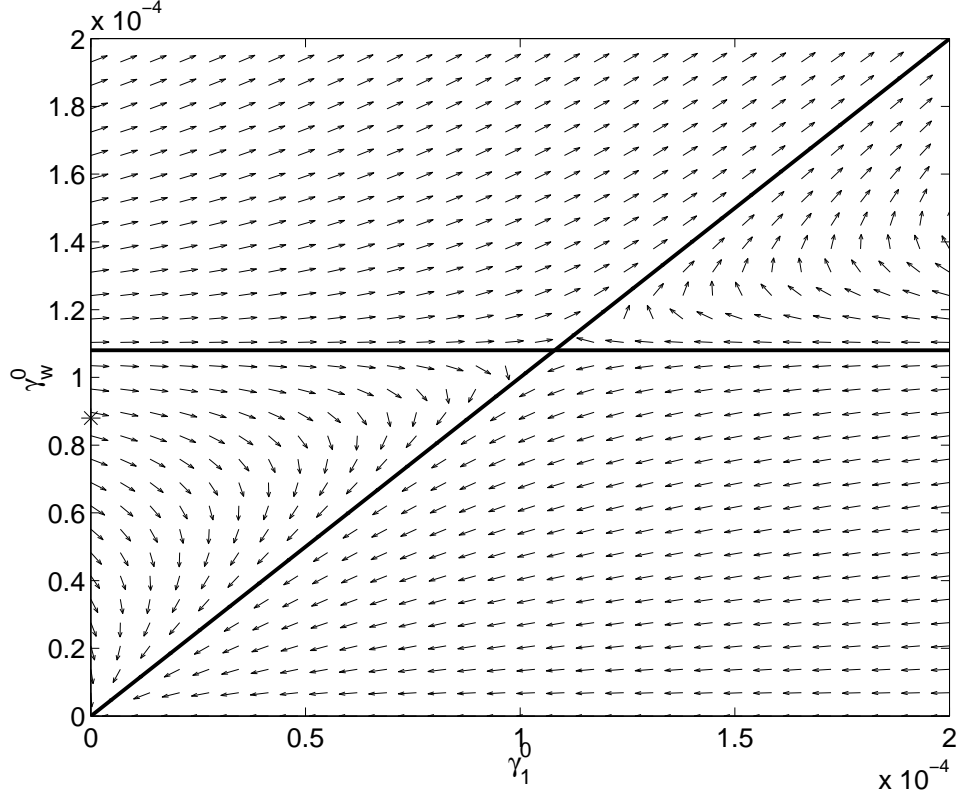


FIG. 13: TIFD projected onto the γ_1 – γ_w plane, where $\gamma_l^0 = 0$ for all l except γ_w^0 and γ_1^0 . The arrows represent the vector field flow $\Gamma^L(\vec{\gamma}) - \Gamma^{L-1}(\vec{\gamma})$. The thick lines illustrate the separatrices. The asterisk marks the fault-tolerance threshold.

To further confirm the results found using the semi-analytical map, we use a Monte-Carlo simulation to determine pseudothresholds for the $[[7,1,3]]$ code. We find the following pseudothresholds with the axis setting by fitting a quadratic to the numerical TRIPS: $\gamma_1^1 \approx 2.3 \times 10^{-1}$, $\gamma_2^1 \approx 2.0 \times 10^{-3}$, and $\gamma_w^1 \approx 2.2 \times 10^{-4}$. We do not expect close agreement for the γ_1^1 pseudothreshold because its value is orders of magnitude above threshold. However, the γ_2^1 and γ_w^1 pseudothresholds found using the flow map differ by no more than a factor of 2 from numerical calculations. This factor could be reclaimed by revisiting some of the approximations in the flow map derivation.

While we do not prove our conjecture, we offer two supporting observations. The first is an observation that follows from the fact that the flow map has a threshold. There are positive integers A and t such that $\Gamma_\ell(\vec{\gamma}) \leq A\gamma_{max}^{t+1}$ for all ℓ , where $\gamma_{max} \equiv \max \gamma_\ell$. These integers determine the well-known lower bound $A^{-1/(t+1)} \equiv \gamma_{th}^{min} \leq \gamma_{th}$ on the threshold.

The next observation is that if Γ causes all components of $\vec{\gamma}$ to increase or remain unchanged, then $\vec{\gamma}$ is above the established lower bound γ_{th}^{min} . More precisely, if $\Gamma_\ell(\vec{\gamma}) \geq \gamma_\ell$ for all ℓ , then $\gamma_\ell \geq \gamma_{th}^{min}$ for at least one ℓ . This is true because if $\gamma_\ell < \gamma_{th}^{min}$ for all ℓ , then $\gamma_{max} < \gamma_{th}^{min}$. In particular, $\Gamma_\ell((\gamma_{max}, \gamma_{max}, \dots, \gamma_{max})) \leq A\gamma_{max}^{t+1} < \gamma_{max}$.

A $\vec{\gamma}$ satisfying the second observation is not necessarily above threshold, but we conjecture that this second observation remains true when γ_{th}^{min} is replaced by γ_{th} for maps Γ describing failure probabilities under independent stochastic error models. We know this to be the case for one-dimensional maps. If the conjecture is true in general, then the level-1 pseudothreshold for the axis setting upper bounds γ_{th} .

VI. CONCLUSIONS AND FUTURE WORK

Pseudothresholds are the failure probabilities below which recursive simulation improves the reliability of a particular component. Yet, pseudothresholds can be much different than the asymptotic threshold. This comes as a surprise not only because it defies the fault-tolerance equation, but because it is a generic phenomenon in both classical and quantum fault-tolerance.

We have shown the difference between pseudothresholds and the asymptotic threshold for classical TMR fault-tolerance. In the quantum setting, we have distinguished pseudothresholds from the fault-tolerance threshold and shown the difference can be up to an order of magnitude. The tools we have presented provide visualization of pseudothresholds and we conjecture that for a given setting, they may provide an upper bound on the fault-tolerance threshold.

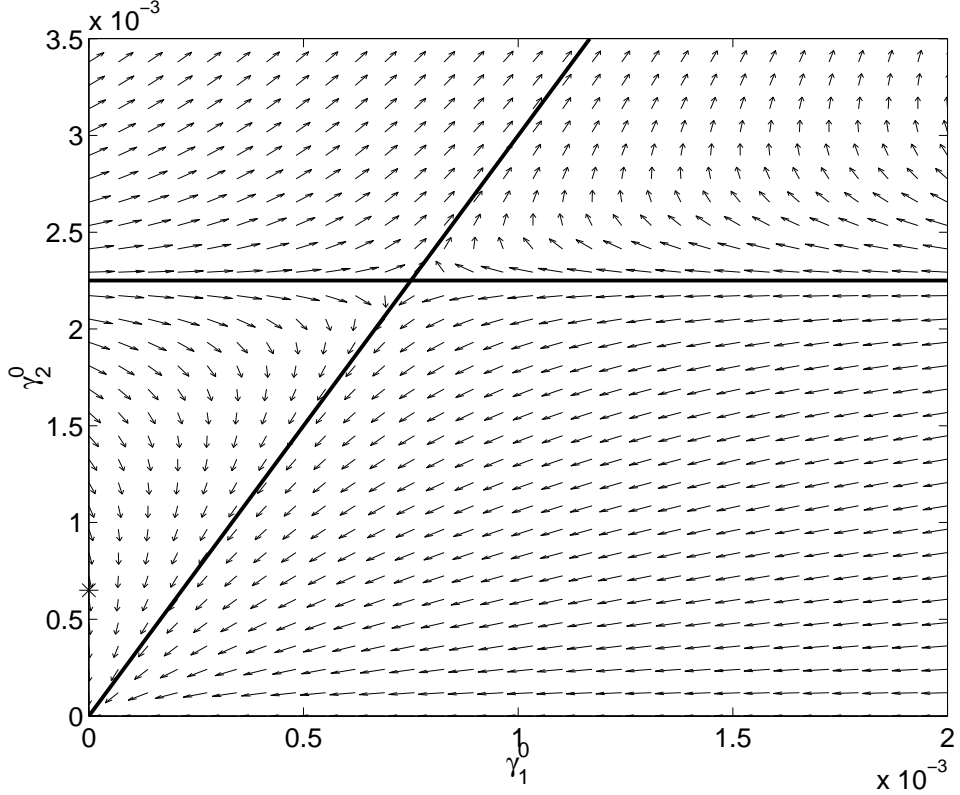


FIG. 14: TIFD projected onto the γ_1 – γ_2 plane, where $\gamma_l^0 = 0$ for all l except γ_1^0 and γ_2^0 . The arrows represent the vector field flow $\Gamma^L(\vec{\gamma}) - \Gamma^{L-1}(\vec{\gamma})$. The thick lines illustrate the separatrices. The horizontal separatrix appears to have zero slope, but it intersects the γ_1^0 -axis at about 10^{-2} . We do not show this intersection because the intersection with the γ_2^0 -axis at about 2.3×10^{-3} has a more significant role in determining the threshold. The asterisk marks the fault-tolerance threshold.

The pseudothreshold problem also casts doubt on the accuracy of some quantum threshold estimates. If some of the reported threshold estimates are actually pseudothresholds, the examples we have given suggest that these estimates may be inaccurate by a factor of 10 or more. These observations apply, in particular, to some of the recent threshold estimates of $O(10^{-3})$ or better. However, by making a judicious choice of concatenation level and setting, the difference between these estimates and an asymptotic threshold can be reduced.

Although a fault-tolerance threshold for infinite scalability cannot be determined by low-level pseudothresholds, pseudothresholds will become important design parameters in engineering a quantum computer. In practice, quantum computers may operate very close to threshold and require only a few levels of recursive simulation. If this is the case, then pseudothresholds can help determine design tradeoffs and the required relative reliability of circuit components. In addition, the difference between pseudothresholds can be used to determine an appropriate level of concatenation that is within current physical capabilities.

This work can be extended in several directions. First, we have put forward a conjecture that pseudothresholds may lead to upper bounds on γ_{th} . If this conjecture is true, then it would be interesting to determine how the concatenated flow equation formalism could be modified to give rigorous bounds. It would also be useful to determine how much a pseudothreshold can differ from the fault-tolerance threshold.

Second, the analyses presented here only account for Clifford group gates. We did not analyze a Toffoli, $\pi/8$, or other nontrivial gate needed for computational universality. It is still possible to apply the methods in this paper to those gates, but the corresponding flow map component is more difficult to estimate well. To determine a quantum fault-tolerance threshold, it is necessary to evaluate a computationally universal basis. With a universal basis, how much does the fault-tolerance threshold and sequence of pseudothresholds change?

A final challenge is to reanalyze the recent threshold estimates by Knill that place the threshold around 10^{-2} [11]. These threshold estimates may indeed differ from the asymptotic threshold by an order of magnitude or more. Evaluating the sequence of pseudothresholds for Knill's fault-tolerance scheme based on quantum teleportation will help determine the accuracy required by a physical device.

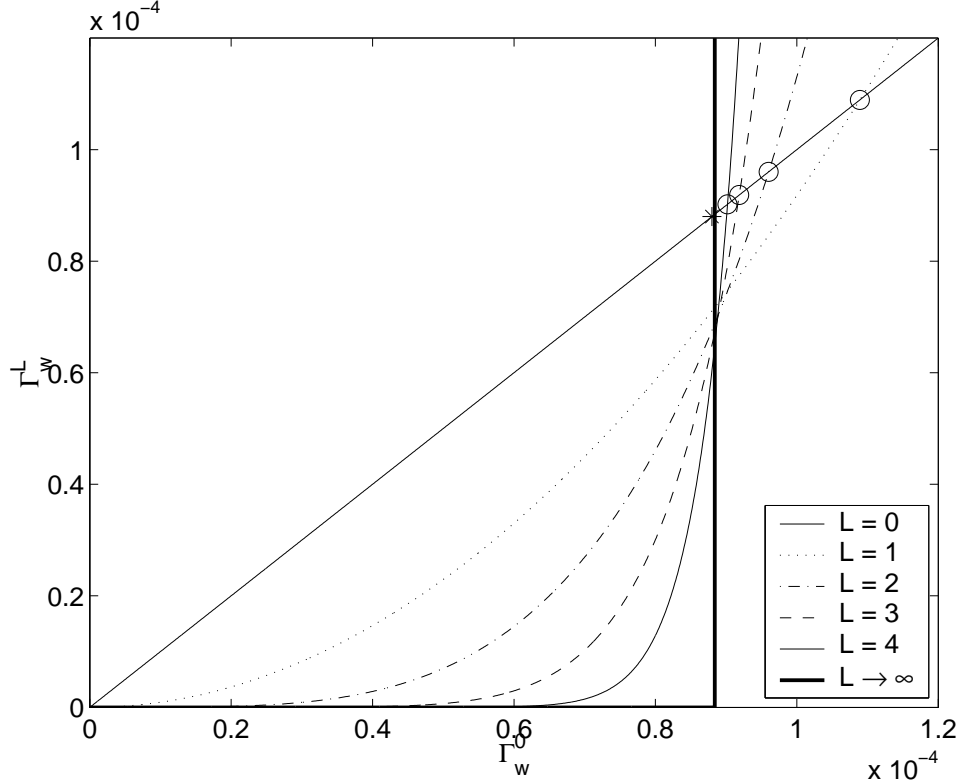


FIG. 15: TRIP for a wait location for $L = 0, 1, 2, 3, 4, \infty$ for the axis setting.

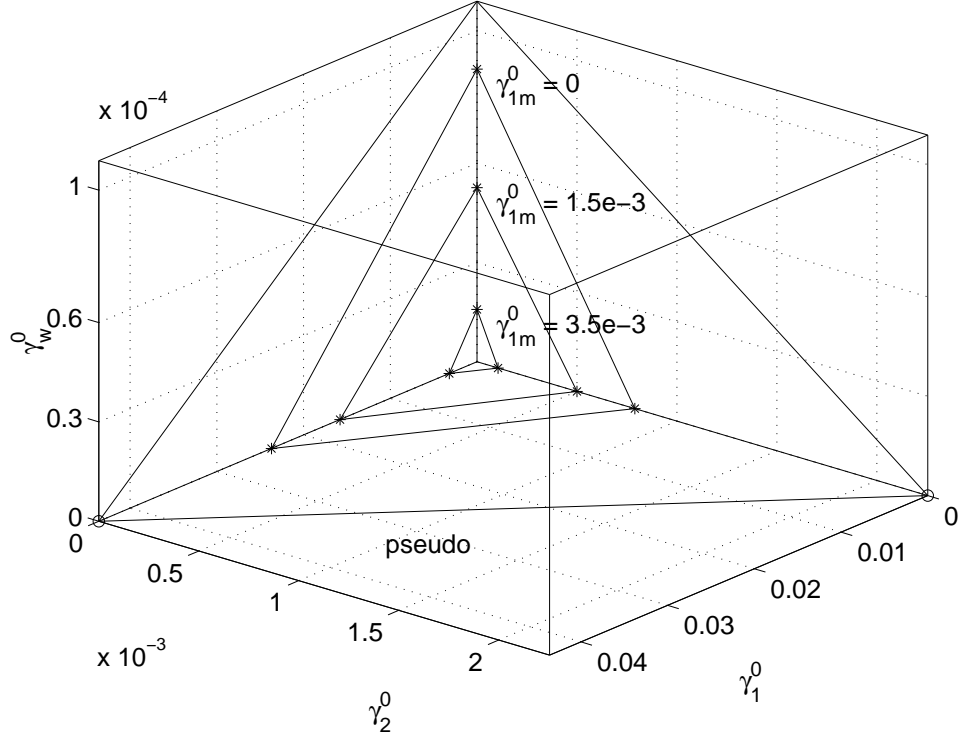


FIG. 16: The set T for the $[[7, 1, 3]]$ code together with a slice of the convex hull of the level-1 axis pseudothresholds. The level-1 axis pseudothresholds are plotted with open circles and connected with lines to illustrate their convex hull. The other three hulls are schematic representations of the numerically computed boundary of the set T for varying values of γ_{1m}^0 . All points beneath a given hull are below threshold. The largest cube contained in T has edge length $\gamma_{th} \approx 8.8 \times 10^{-5}$.

VII. ACKNOWLEDGEMENTS

Krysta Svore acknowledges support from an NPSC fellowship. Andrew Cross acknowledges support from an NDSEG fellowship.

- [1] P. W. Shor. Algorithms for quantum computation: discrete logarithms and factoring. In *35th Annual Symposium on Foundations of Computer Science, Proceedings*, pages 124–134. IEEE, IEEE Press, 1994.
- [2] L. K. Grover. Quantum mechanics helps in searching for a needle in a haystack. *Phys. Rev. Lett.*, 79:325, 1997. quant-ph/9706033.
- [3] S. Hallgren. Polynomial-time quantum algorithms for Pell’s equation and the principal ideal problem. In *Proceedings of the Thirty-Fourth Annual ACM Symposium on Theory of Computing*, pages 653–658, 2002.
- [4] J. von Neumann. Probabilistic logics and the synthesis of reliable organisms from unreliable components. In *Automata Studies*, pages 328–378. Princeton University Press, 1956.
- [5] J. Preskill. Fault-tolerant quantum computation. In H. Lo, S. Popescu, and T. Spiller, editors, *Introduction to quantum computation and information*. World Scientific Publishing Company, 2001. quant-ph/9712048.
- [6] K. Svore, B. Terhal, and D. DiVincenzo. Local fault-tolerant quantum computation. *To appear in Phys. Rev. A*, 2005. quant-ph/0410047.
- [7] D. Aharonov and M. Ben-Or. Fault-tolerant quantum computation with constant error. *Proceedings of the 29th Annual ACM Symposium on the Theory of Computation*, pages 176–188, 1997. quant-ph/9906129.
- [8] E. Dennis, A. Kitaev, A. Landahl, and J. Preskill. Topological quantum memory. *J. Math. Phys.*, 43:4452–4505, 2002. quant-ph/0110143.
- [9] D. Gottesman. *Stabilizer codes and quantum error correction*. PhD dissertation, Caltech, 1997. quant-ph/9705052.
- [10] E. Knill, R. Laflamme, and W. Zurek. Resilient quantum computation: Error models and thresholds. *Science*, 279(5349), 1998. quant-ph/9702058.
- [11] E. Knill. Quantum computing with realistically noisy devices. *Nature*, 434:39–44, 2005. quant-ph/0410199.
- [12] T. Ohno, G. Arakawa, I. Ichinose, and T. Matsui. Phase structure of the random-plaquette Z_2 gauge model: accuracy threshold for a toric quantum memory. *Nuclear Physics B*, 697:462–480, 2004. quant-ph/0401101.
- [13] B. Reichardt. Improved ancilla preparation scheme increases fault-tolerant threshold. *Unpublished*, 2004. quant-ph/0406025.
- [14] M. Silva, M. Rötteler, and C. Zalka. Thresholds for linear optics quantum computing with photon loss at the detectors. *Unpublished*, 2005. quant-ph/0502101.
- [15] A. M. Steane. Overhead and noise threshold of fault-tolerant quantum error correction. *Phys. Rev. A*, 68(042322), 2003. quant-ph/0207119.
- [16] C. Zalka. Threshold estimate for fault tolerant quantum computing. *Unpublished*, 1996. quant-ph/9612028.
- [17] P. Aliferis, D. Gottesman, and J. Preskill. Quantum accuracy threshold for concatenated distance-3 codes. *Unpublished*, 2005. quant-ph/0504218.